Journal of Hazardous Materials 416 (2021) 126237

Contents lists available at ScienceDirect

Journal of Hazardous Materials

journal homepage: www.elsevier.com/locate/jhazmat

Research Paper

# Smart hydrogel-microsphere embedded silver nanoparticle catalyst with high activity and selectivity for the reduction of 4-nitrophenol and azo dyes

Dambarudhar Parida [a,*], Eva Moreau [a], Rashid Nazir [a], Khalifah A. Salmeia [b], Ruggero Frison [c], Ruohan Zhao [a], Sandro Lehner [a], Milijana Jovic [a], Sabyasachi Gaan [a,*]

[a] Advanced Fibers, Empa, Swiss Federal Laboratories for Materials Science and Technology, St Gallen CH-9014, Switzerland
[b] Department of Chemistry, Faculty of Science, Al-Balqa Applied University, 19117 Al-Salt, Jordan
[c] Center for X-Ray Analytics, Empa, Swiss Federal Laboratories for Materials Science and Technology, Dubendorf CH-8600, Switzerland

ARTICLE INFO

Editor: Dr. L. Haizhou

*Keywords:*
Silver nanoparticles
Responsive hydrogel
Nanocomposite
4-Nitrophenol reduction
Selective catalysis

ABSTRACT

A simple method is reported for the preparation of silver nanoparticle (AgNP) embedded pH-responsive hydrogel microparticle catalyst via Michael addition gelation and in-situ silver nitrate ($AgNO_3$) reduction. The AgNP-hydrogel microsphere exhibited an efficient reduction of pollutants like 4-Nitrophenol (4-NP) and Congo red (CR) under acidic medium with turn over frequency (TOF) of ~170 $h^{-1}$ and ~124 $h^{-1}$ respectively. Interestingly, the activity of the catalysts was turned-OFF under a basic medium ($\geq$ pH 12) due to the deswelling pH-responsive matrix surrounding the AgNPs. On the contrary, turning-OFF the hydrogenation of a cationic pollutant like methylene blue (MB) using high pH ($\geq$ 12) was not possible, due to ionic interaction of MB molecules with the negatively charged catalyst at this pH. This feature was used to demonstrate selective hydrogenation of only MB from a mixture of 4-NP and MB. Finally, five recycling steps confirmed the reusability and practical application potential of the catalyst.

## 1. Introduction

Accumulation of degradation-resistant pollutants such as nitro-aromatics and azo dyes in water bodies poses a threat to the aquatic ecosystem as well as human health. The high water solubility of certain nitroaromatics like 4-nitrophenol (4-NP) and azo dyes can make their removal quite challenging. This triggered the development of methods based on efficient adsorbents (Yagub et al., 2014; Gupta et al., 2013; Dias and Petit, 2015; Parida et al., 2021), photocatalytic degradation (Dias and Petit, 2015), bio-degradation (Marvin-Sikkema and de Bont, 1994; Ju and Parales, 2010), and catalytic conversion (Fu et al., 2019; Zeng et al., 2013) as viable purification strategy to maintain good water quality. Among these options, catalytic conversion is the preferred method as it offers a possibility to convert the pollutants to valuable products and less harmful counterparts with high efficiency. For example, upon hydrogenation, carcinogenic 4-NP can be converted to 4-aminophenol (4-AP), which is an intermediate for corrosion inhibitors (Thenmozhi et al., 2014; Guenbour et al., 2000), pharmaceutical molecules, and dyes (Buschmann, 2007). Transforming nitro pollutants to useful amino compounds is a green and commercially beneficial approach to get rid of pollutants.

Among various methods, noble metal nanoparticles (NMPs) catalyzed hydrogenation continues to draw considerable attention owing to their high activity and oxidative stability (Fu et al., 2019; Zheng and Zhang, 2007; Qin et al., 2019; Lu et al., 2006; Soğukömeroğulları et al., 2019; Kästner and Thünemann, 2016). With the rise in demand for active catalysts, the use of noble metals like Au, Pt, and Pd-based catalysts have grown recently (Fu et al., 2019; Soğukömeroğulları et al., 2019; Ansar and Kitchens, 2016; Nguyen et al., 2019; Sun et al., 2014; Johnson et al., 2013; Goepel et al., 2014; Fu et al., 2019). However, the high cost of these metals is a major drawback and thus triggered the development of supports for enhanced recoverability. Supports containing magnetic particle is one such approach for easy recovery and reuse of expensive NMP catalysts (Zeng et al., 2013; Yang et al., 2020; Xu et al., 2020). The development of bimetallic nanoparticle catalysts is another approach to reduce the cost along with improvement in the activity compared to their monolithic counterparts (Qin et al., 2019; Fu et al., 2018). Despite these attempts, the overall price of such catalysts remains higher than catalysts prepared from metals like Ni, Cu, and Ag.

In this context, MNPs of moderately active and low-cost metals (Cu

* Corresponding authors.
*E-mail addresses:* dambarudhar.parida@empa.ch (D. Parida), sabyasachi.gaan@empa.ch (S. Gaan).

https://doi.org/10.1016/j.jhazmat.2021.126237
Received 9 February 2021; Received in revised form 6 May 2021; Accepted 24 May 2021
Available online 26 May 2021
0304-3894/© 2021 The Author(s). Published by Elsevier B.V. This is an open access article under the CC BY license (http://creativecommons.org/licenses/by/4.0/).

and Ag) are still attractive choices as catalysts (Li et al., 2015; Zhou et al., 2020; Das et al., 2019; Dong et al., 2014; Qian et al., 2020; Bhaduri and Polubesova, 2020; Sudhakar and Soni, 2018; Budi et al., 2021). To improve the activity of silver nanoparticles (AgNPs), supports have been designed to boost the catalytic activity via increasing the available surface area for catalysis. Using this principle, nanosheets (Li et al., 2015; Qian et al., 2020; Mao et al., 2018), conductive polymers (Das et al., 2019), and fibrous silica (Dong et al., 2014) were employed for the successful enhancement of the catalytic activity of AgNPs. On the other hand, porous supports prepared from carbon and organic polymers are also known to have a positive effect on the catalytic activity of NMPs (Zhou et al., 2020; Bhaduri and Polubesova, 2020; Gong et al., 2019; Xia et al., 2016; Budi et al., 2020). In the case of these supports, confined space reaction and enrichment of micro-environment abound NMPs by adsorption of substrate molecules enhance the activity (Qin et al., 2019; Gong et al., 2019; Cárdenas-Lizana et al., 2013). Moreover, fast electron transfer from support like carbon black to NMPs is also known to improve catalytic efficiency (Qin et al., 2019). Although these supports are known to enhance the catalytic activity of NMP, a portion of the NMP surface is shielded by the support, thus, resulting in their underutilization.

To counter the underutilization of NMPs, relatively mobile cross-linked polymeric networks or hydrogels are investigated as supports (Lu et al., 2006; Li et al., 2010, 2011; Wang et al., 2010; Irene, 2018; Begum et al., 2019). These supports allow easy access to the NMP surface along with substrate and product exchange. Such polymeric supports also facilitate tuning the catalytic activity via an external stimulus such as temperature, pH, and salt concentration (Lu et al., 2006; Li et al., 2010; Li et al., 2011; Wang et al., 2010; Irene, 2018). However, complicated preparation methods of such stimuli-responsive catalysts make them unattractive (Li et al., 2010; Li et al., 2011). Lack of complete control over activity also hinders the wide acceptability of such responsive catalysts (Lu et al., 2006; Kästner and Thünemann, 2016; Li et al., 2011; Irene, 2018). Considering the potentials of responsive supports, a simplified method needs to be developed to improve the catalytic activity, controllability, and selectivity of embedded NMPs.

Herein, a simple water-in-oil emulsion route is reported for the preparation of AgNP embedded responsive hydrogel microsphere catalyst. Such catalyst was prepared by the emulsification of an aqueous solution of Trivinylphosphine oxide (TVPO), Piperazine, and $AgNO_3$ followed by simultaneous Michael addition crosslinking of TVPO-Piperazine and simultaneous in-situ formation of AgNPs within the emulsified micro-droplets. The composite microspheres were characterized by X-Ray diffraction (XRD), Scanning electron microscopy (SEM), and X-ray photoelectron spectroscopy (XPS). Dynamic light scattering (DLS) analysis confirmed the pH-responsive behavior of the composite hydrogel-microsphere. pH-responsive swelling-deswelling of the composite microsphere was utilized to control the access to AgNPs and modulate their catalytic activity (Fig. 1). This feature was investigated using 4-NP, Congo red (CR), and Methylene blue (MB) as model pollutants. Switching ON-OFF of the catalytic activity was demonstrated by changing the pH of the reaction medium. Substrate selectivity of the novel catalyst was also investigated using a mixture of 4-NP and MB. Finally, the reusability of the catalysts was demonstrated to highlight their practical application potential.

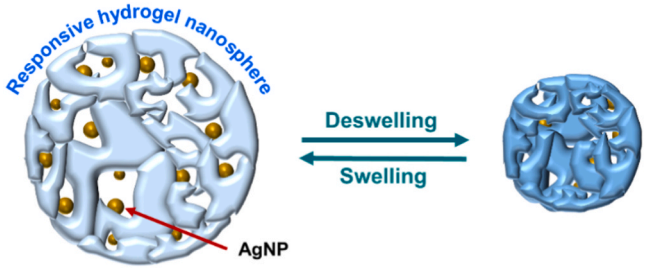


**Fig. 1.** Synthesis of AgNPs few nanometers below the surface hydrogel-microsphere and controlling the access to AgNP surface by swelling-deswelling.

## 2. Materials and method

### 2.1. Materials

$AgNO_3$ (≥ 99.0%), Sodium borohydride ($NaBH_4$), MB, CR, 4-NP, Phosphoryl trichloride, vinyl magnesium bromide (1 M in THF), dry THF, piperazine, and Span 80 were purchased from Sigma-Aldrich and used as received. Trivinylphosphine oxide (TVPO) was synthesized by a reported procedure and confirmed by NMR analysis (Nazir et al., 2020b).

### 2.2. Hydrogel and in-situ AgNP synthesis

#### 2.2.1. Hydrogel preparation

Hydrogel was prepared by Michael addition of TVPO (64.0 mg, 0.50 mmol) and piperazine (64.6 mg, 0.75 mmol) in 2.5 mL of water (40 °C for 16 h) (Nazir et al., 2020b). pH-responsive swelling of the transparent hydrogel was determined by measuring the swelling ratio (SR) by the procedure reported in our previous publication (Nazir et al., 2020b) and details can also be found in Sec. S1.1.

#### 2.2.2. In-situ AgNP-hydrogel preparation

2, 5, and 10.5 mol% of $AgNO_3$ was added to 2.5 mL aqueous solution of TVPO (64.0 mg) and piperazine (64.6 mg) kept in an ice bath. The solutions were then transferred to cuvettes, sealed, and transferred to an oven (at 40 °C). All operations were carried out in dark and separate cuvettes were used for each duration. UV–vis spectra of solutions were recorded at intervals.

### 2.3. Synthesis of AgNPs containing hydrogel-microspheres

#### 2.3.1. Amine mediated in-situ method (Method 1)

For the preparation of the responsive catalyst, the process was developed to prevent the AgNP formation on the surface of microspheres. Therefore, $AgNO_3$ was not premixed with the Michael adducts, rather it was added after the initiation of gelation. As shown in Fig. 2a, 0.5 g of Span 80 was mixed with 20 mL of cyclohexane using Ultraturax (19,000 rpm, 5 min). Then, a freshly prepared 5 mL aqueous solution of TVPO (128 mg, 1 mmol) and piperazine (129.2 mg, 1.5 mmol) was added dropwise to this mixture under stirring (19,000 rpm) to obtain a milky emulsion. Then, the centrifuge tube was covered with aluminum foil and transferred to a water bath under stirring (40 °C, 500 rpm). After 15 min, 0.1 mL aqueous solution of $AgNO_3$ (48 mg/mL) was added to the emulsion and stirred for 16 h to obtain a light brown emulsion (Fig. S2). Then, the emulsion was dialyzed (24 h) using ethanol as dialysate and 15 KD RC dialysis tubes. The dialysate was replaced 3 times followed by dialysis in deionized water (24 h) to replace ethanol with water. This sample is named **E1** (Fig. 2a) and the emulsion prepared without the addition of $AgNO_3$ is named **E0**.

#### 2.3.2. $H_2$-assisted in-situ method (method 2)

Emulsion of TVPO (128 mg, 1 mmol) and piperazine (129.2 mg, 1.5 mmol) was prepared in a pressure reactor by the procedure as described in Section 2.3.1, and the pressure reactor was transferred to a water bath at 40 °C under stirring (15 min). 0.1 mL aqueous solution of $AgNO_3$ (48 mg/mL) was added to the emulsion and stirred for 2 h (Fig. 2b). Then, the reactor was pressurized with $H_2$ (~2.5 bar) and the stirring was continued for 14 h at 40 °C. The emulsion was then purified by dialysis as reported in Method 1 and the sample was named **E2**.

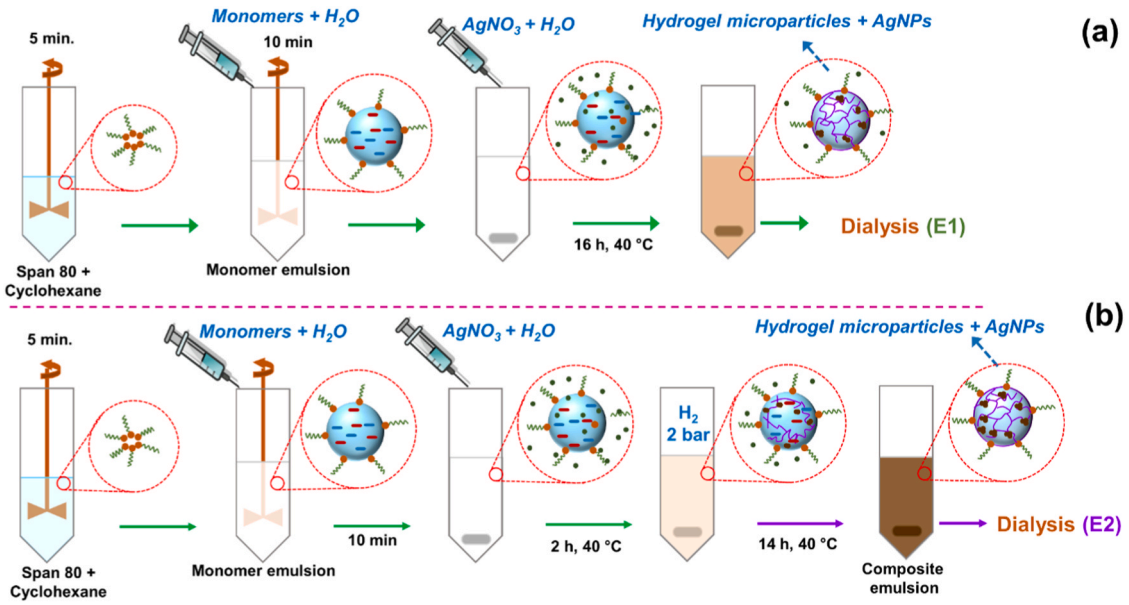


**Fig. 2.** Preparation of hydrogel-microsphere embedded AgNPs catalyst by (a) amine mediated in-situ and (b) $H_2$-assisted in-situ method.

### 2.4. Characterizations of composite microspheres

#### 2.4.1. UV–vis analysis

UV–vis spectra for in-situ AgNP formation and catalytic reaction were recorded using a Varian Cary 50 UV–Vis Spectrophotometer. Catalytic reduction of 4-NP, MB, and CR were analyzed by recording the UV–vis spectra of the reaction solution as a function of time and the residual concentration was determined using their corresponding UV–vis calibration curves.

#### 2.4.2. Nuclear magnetic resonance (NMR) analysis

NMR analysis was carried out Bruker AV-III 400 NMR spectrometer (Bruker Biospin AG, Fällanden, Switzerland). The $^{1}H$, $^{13}C$, and $^{31}P$ NMR spectra were recorded using Bruker standard pulse on a 5 mm Cryo-Probe™ equipped with z-gradient employing 90° pulse lengths of 11.4 μs ($^{1}H$), 10.0 μs ($^{13}C$), and 16.0 μs ($^{31}P$).

#### 2.4.3. Inductively coupled plasma optical emission spectrometry (ICP-OES) analysis

ICP-OES analysis was used to determine the silver content (Ag-content) of samples. ICP-OES 5110 (Agilent, Basel, Switzerland) apparatus was used for these experiments. Samples preparation for ICP-OES consisted of mixing 10 mg of the sample with 3 mL $HNO_3$, followed by the digestion at 250 °C for 30 min using microwave heating.

#### 2.4.4. XRD analysis

XRD analysis was carried out in a Stoe IPDS-II instrument, operating at a voltage of 50 kV and a current of 40 mA with Mo Kalpha radiation ($\lambda = 0.71073$ Å) at an angular range ($2\theta$) of 5–50°. The instrumental contribution was taken into consideration by measuring the diffraction pattern of LaB6 as the reference material and used within Topas software (Coelho, 2018).

#### 2.4.5. DLS analysis

DLS analysis was carried out in a Malvern Zetasizer Nano ZS90 at 25 °C to determine the particle size of hydrogel-microspheres. Before analysis, the pH of the dispersion was adjusted to the desired value and kept for 1 h at 25 °C to achieve an equilibrium swelling. The same samples were used to measure the ζ-potential using folded capillary Zeta Cell DTS1070.

#### 2.4.6. SEM analysis

SEM analysis was carried out in a Hitachi S-4800 SEM equipment operating in scanning and transmission mode (30 kV). For SEM images, samples were prepared by putting a drop of emulsion on a silicon wafer and evaporating the water at room temperature for 16 h followed by 7 nm Au/Pd coating. For transmission images, the sample was prepared by putting a drop of emulsion on a lacey carbon grid and evaporating the water over 16 h at room temperature.

#### 2.4.7. XPS analysis

XPS analysis was carried out on a Physical Electronics (PHI) Quantum 2000 X-ray photoelectron spectrometer equipped with a monochromatized AlKα source (at 15 kV, 28.8 W), and a hemispherical electron energy analyzer fitted with a channel plate and a position-sensitive detector. The sample was analyzed with an electron take-off angle of 45° and spectra were recorded with constant pass energy mode (46.95 eV and energy resolution of 0.95 eV). Spectra were processed with PHI MultiPak.

### 2.5. Catalytic hydrogenation of pollutants

#### 2.5.1. 4-NP hydrogenation

14.4 mg of 4-NP (0.1 mmol) and 35.4 mg of $NaBH_4$ (0.94 mmol) were dissolved in 12.0 mL water (40 °C) maintained at different pH. The reduction was initiated by adding 1.5 mL of **E2** (at the same pH) to the freshly prepared 4-NP-$NaBH_4$ solution under stirring (500 rpm). The reduction of 4-NP was monitored by measuring the UV–vis intensity of 4-NP centered around 400 nm after required dilution. Separate samples were prepared for each duration. TOF of the reaction was calculated as the moles of 4-NP reduced by a mole of Ag-atom in an hour.

#### 2.5.2. CR and MB hydrogenation

For MB hydrogenation, 60 μL of MB solution (10.0 g/L) and $NaBH_4$ (35.4 mg, 0.94 mmol) were added to 12.7 mL of water at desired pH. Then, 0.75 mL of **E2** was added to the solution and the reaction was monitored by UV–vis spectroscopy after required dilution.

For CR reduction, 60 μL of CR solution (20.0 g/L) and $NaBH_4$ (35.4 mg, 0.936 mmol) were added to 12.75 mL of water at desired pH followed by the addition of **E2** (0.75 mL) under stirring. Then the catalytic reduction of CR was monitored by UV–vis spectroscopy. Both MB and CR reduction were carried out at 40 °C and separate samples were

prepared for each duration.

## 3. Result and discussion

### 3.1. In-situ AgNP-hydrogel composites preparation

The hydrogels were synthesized via previously reported Michael addition crosslinking of TVPO and piperazine (at 40 °C) in presence of 2, 5, and 10.5 mol% $AgNO_3$ (Nazir et al., 2020a, 2020b). Colorless solutions turned dark red with time, indicating the formation of AgNPs (Fig. 3 and S1). The appearance of a UV–vis band of nanosilver at $\lambda_{max}$ 380 nm just after 5 min confirmed the formation of $Ag^0$ nuclei at the early stage (Fig. S1d). The redshift of the band with time indicated the growth of nuclei to AgNPs (Agnihotri et al., 2014; Zhao et al., 2013). The presence of $AgNO_3$ led to faster gelation (Fig. S1a-c) and the solution containing 10.5 mol% of $AgNO_3$ formed the gel within 45 min compared to 16 h for pristine hydrogel (at 40 °C). Fast gelation in the case of precursor solution containing $AgNO_3$ can be attributed to physical reasons. In-situ nanoparticle formation (Mishra et al., 2014; Hoogesteijn von Reitzenstein et al., 2016) and crosslinking of precursors lead to a rapid rise in viscosity compared to pristine precursor solution. A combination of these factors reduces the flow behavior and the solutions behave like a hydrogel.

As explained earlier (Fig. 1), the swelling-deswelling behavior of the composite hydrogel is important to control the catalytic activity. As a measure of responsiveness, the swelling ratio (SR) of AgNP-hydrogel composites was determined (Eq.S1, Sec. S1.1). From Fig. 3b it can be seen that a slight decrease in deswelling was observed in composites prepared with 1.0 and 2.0 mol% of $AgNO_3$. However, composite prepared with 10.5 mol% $AgNO_3$ displayed only limited deswelling, which can be attributed to the formation of the rigid matrix due to the presence of a large number of AgNPs. Finally, gel-phase NMR analysis of composite hydrogel (Fig. S2) confirmed the absence of any side reaction in presence of $AgNO_3$. Details of NMR analysis can be found in Sec. S2.

Direct synthesis of AgNP-hydrogel composite from the precursors (TVPO and piperazine, silver salts) has simplified the catalyst preparation. The use of bulk composite as a catalyst can lead to poor catalytic activity due to diffusion limitations. To overcome such drawbacks and facilitate easy access to catalytic sites, the AgNP-hydrogel composite was prepared in the form of microspheres by an emulsion process (Fig. 2). Considering moderate Ag-content and minimum loss in swelling behavior, hydrogel-microspheres were prepared using 2.0 mol% of $AgNO_3$.

### 3.2. Preparation of AgNP embedded hydrogel-microspheres

The absence of AgNPs on the surface of the microsphere is important to achieve complete control over the catalytic activity of AgNPs by swelling-deswelling. Therefore, the method was developed to prevent the formation of AgNPs on the surface of hydrogel-microspheres. Particularly, premixing of $AgNO_3$ with the Michael addition precursors was avoided, rather $AgNO_3$ was added to the emulsion after initiation of gelation within droplets to facilitate the formation of AgNPs a few nanometers below the surface. Hydrogel-microspheres without AgNPs (**E0**) and with AgNPs (**E1**) were prepared by this method (Section 2.3.1). The light brown color of **E1** indicates the presence of AgNPs within microspheres (Fig. S3). The solid content of the purified **E1** in water was found to be 0.9% with an Ag-content of ~0.35 wt% on dried **E1** (Table S1), which is significantly lower than the calculated Ag-content of 1.1%. This can be attributed to the fast gelation of Michael precursors within the droplets. This leads to the formation of tertiary amines before the complete reduction of $AgNO_3$. The reduction potential of tertiary amines is known to be lower than the secondary amines (Piao et al., 2011). As a result, unreduced $AgNO_3$ is removed from **E1** during the subsequent purification step.

To enhance the Ag-content in the hydrogel-microspheres, $H_2$ was introduced in the reactor (~2.5 bar) 2 h after the addition of $AgNO_3$ (**E2,** Fig. 2b), and the emulsion was stirred for a further 14 h. $H_2$-assisted method (**E2**) resulted in a much darker emulsion than **E1** (Fig. S3), indicating higher Ag-content in **E2**. UV–vis spectra of purified **E0**, **E1,** and **E2** were recorded after equal dilution in water (Fig. 4a). In the case of **E0**, UV-absorption was observed only below 320 nm, which is consistent with our previous report (Nazir et al., 2020b). This makes easy detection of embedded AgNPs within **E1** and **E2** hydrogel microspheres. The absorption band of AgNPs was visible at ~415 nm (Parida et al., 2020; Sirohi et al., 2019), owing to the transparency of the hydrogel matrix within this wavelength range. The higher intensity of the band at 415 nm for **E2** indicates a higher concentration of AgNPs within microspheres.

The formation of AgNPs within microspheres was also confirmed by powder XRD of dried **E1** and **E2** (Fig. 4b). Diffused diffraction pattern of hydrogel (**E0**) was present in the XRD patterns of both **E1** and **E2**. Diffraction peaks at 2θ of 17.7°, 20.4°, 29.0° and 33.5° in case of **E1** and **E2** can be assigned to (111), (200), (220), and (310) reflections of a face-

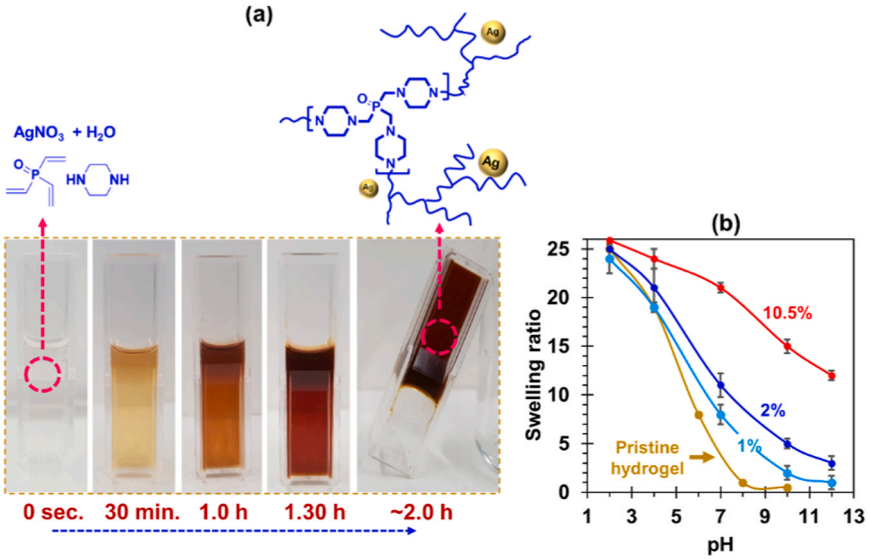


**Fig. 3.** (a) Change in color of precursor solution containing 2% $AgNO_3$ (at 40 °C) indicates the in-situ formation of AgNPs. AgNP synthesis at different $AgNO_3$ loading is given in Fig. S1. (b) Swelling ratio of pristine and composite hydrogels prepared using different $AgNO_3$ loading.

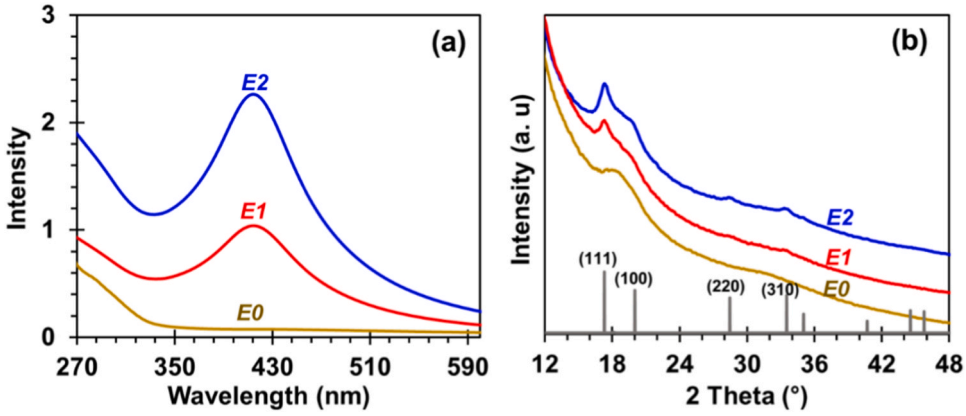


**Fig. 4.** (a) UV–vis spectra of hydrogel-microspheres with and without AgNPs (**E0**, **E1**, and **E2**) at the similar concentration (b) XRD patterns of dried **E0**, **E1**, and **E2**.

centered cubic $Ag^0$ crystals (Parida et al., 2020). The size of AgNPs determined using 111-plane was found to be ~8 nm for both **E1** and **E2**. Then, Ag-content in dried **E2** was found to be 0.7 ± 0.04 wt%, which is close to the calculated value (i.e. 1.1%, Table S1). Therefore, only **E2** was selected for further characterization and catalytic study. From the solid content and ICP-OES analysis (Table S1), the Ag-content of **E2** was calculated to be 0.059 mg/mL.

### 3.3. Characterization of AgNP embedded hydrogel-microspheres

The pH responsiveness of **E2** was determined by DLS analysis at different pH values. At pH 4, the particle size was 980 nm and ζ-potential of + 34 mV indicates its good dispersion stability at this pH (Fig. 5a, Table 1). A decrease in the particle size (807 nm) and ζ-potential (+13 mV) was observed with an increase in the pH to 7. This led

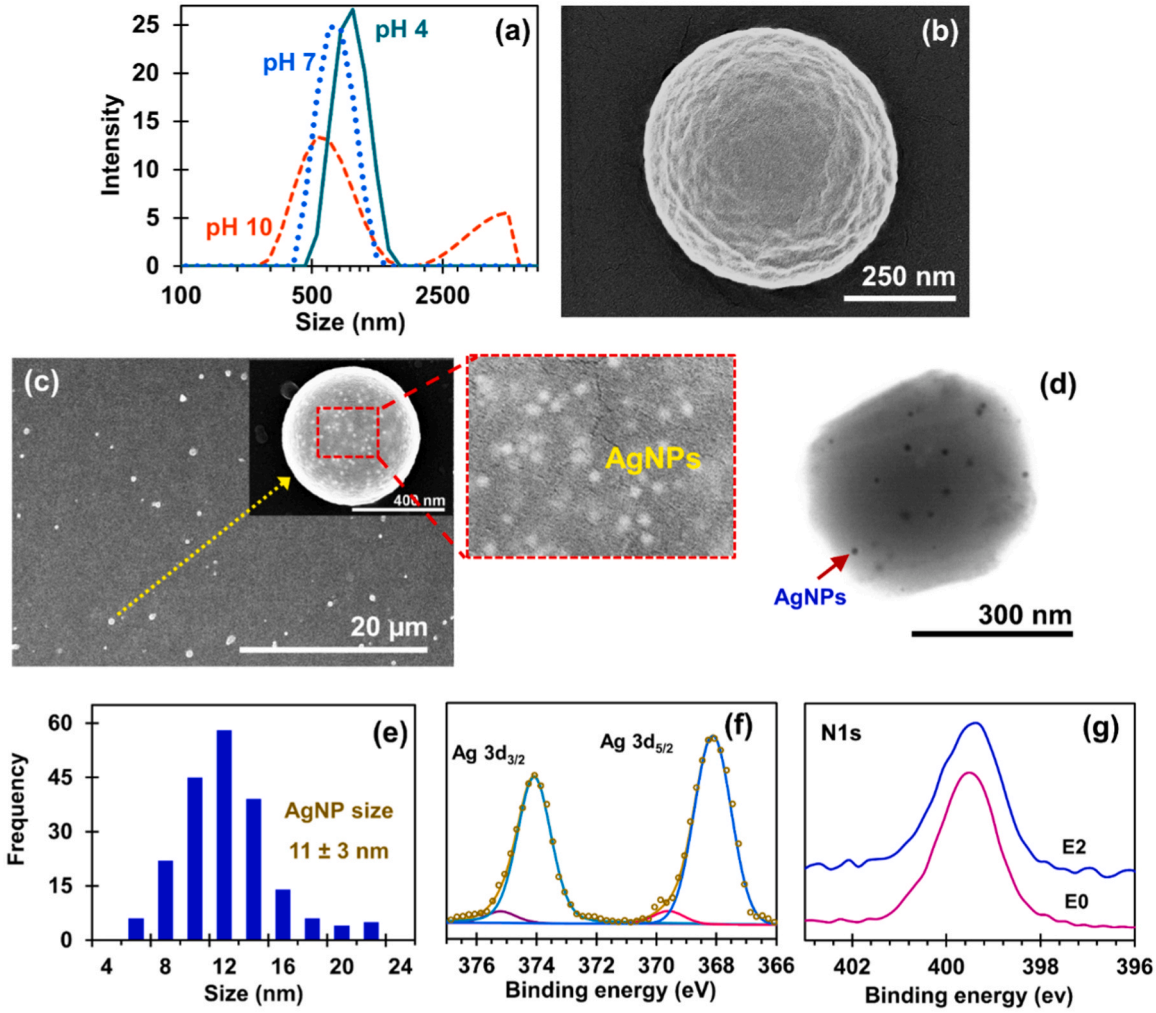


**Fig. 5.** (a) DLS particle size of **E2** at different pH. SEM image of (b) **E0** and (c) **E2**. The enlarged view of the **E2** surface showing the presence of AgNPs with few nanometers within the surface (d) SEM image of **E2** under transmission mode (more images in Fig. S5). (e) Size histogram of AgNPs in **E2**. (f) Deconvoluted high-resolution XPS scan of **E2** in the region of Ag. (g) High-resolution XPS scan in the N1s region of **E0** and **E2**.

**Table 1**
Particle size and ζ-potential of **E2** at different pH.

| pH | Particle size (nm) | ζ-potential (mV) |
|---|---|---|
| 4 | 980 | +34 |
| 7 | 807 | +13 |
| 10 | – | -6 |
| 12 | – | – |

Note: blank space in case of pH 10 and 12 indicate unreliable values due to precipitation of microspheres.

to poor dispersion stability of **E2** and precipitation after ~2 h (Fig. S4). To compare the swelling behavior of **E2** with the bulk composite hydrogel, the ratio of particle volume at pH 4 and pH 7 ($V_{pH4}/V_{pH7}$) was calculated using the average particle size obtained in DLS experiments. $V_{pH4}/V_{pH7}$ of **E2** was found to be 1.8, which is in agreement with the ratio of SR of the bulk hydrogel at pH 4 and pH 7 ($SR_{pH4}/SR_{pH7}$ =1.9).

Increasing the pH to 10 resulted in a decrease of the ζ-potential to − 6 mV (Table 1), indicating the unstable nature of the dispersion (Fig. S4), and two populations of particles were observed during DLS analysis (Fig. 5a). Although the decrease in particle size of **E2** is expected at pH 10, the larger particle size observed at this pH is due to the aggregation of smaller particles. Two particle populations make it difficult to compare the change in volume at pH 10 (Fig. 5a). Further increasing the ≥ pH 12, an extensive aggregation was observed with unreliable DLS results.

SEM analysis of **E2** was carried out both in scanning and transmission mode to determine the location of AgNPs in microspheres. As expected, no sign of AgNPs was observed during SEM analysis of **E0** (Fig. 5b). SEM images of **E2** showed the presence of AgNPs a few nanometers below the surface of the microsphere (Fig. 5c). Transmission images also confirmed the presence of AgNPs (13 ± 3 nm, Fig. 5d, and e) few nanometers within the microsphere. The size of AgNPs determined by transmission images was found to agree with XRD analysis (~8 nm). It is worth mentioning here that, absence of AgNPs on the surface of microspheres prevents any catalytic activity at its deswollen state, which offers excellent control over the activity just by swelling and deswelling of the **E2**.

XPS analysis was carried out to determine the oxidation state of the silver in **E2** (Sirohi et al., 2019; Ruíz-Baltazar et al., 2018; Cheng et al., 2015). The high-resolution scan in Fig. 5f shows the presence of two peaks between 365 and 377 eV due to spin-orbital splitting to Ag $3d_{5/2}$ and Ag $3d_{3/2}$ core levels. Both the peaks can be resolved into two components, with major peaks at 368.2 ($3d_{5/2}$) and 374.2 eV ($3d_{3/2}$) assigned to $Ag^0$. The small peaks at 369.6 and 375.3 eV were assigned to oxidized silver ($Ag^+$). Based on the peak area, the $Ag^0$ component was found to be ~95%. Analyzing the N1s spectra, an overall shift towards lower binding energy was observed in **E2** as compared to **E0** (Fig. 5g). This can be attributed to an increased number of secondary amines in **E2** than **E0**, which is in agreement with the NMR analysis. Analysis of N1s spectra confirms the absence of any AgNPs-hydrogel chemical interactions, and AgNPs are physically stabilized within the hydrogel.

### 3.4. Catalytic activity determination

#### 3.4.1. Reduction of 4-NP

To study the possible reduction of 4-NP in the absence, aqueous solutions of 4-NP and $NaBH_4$ at different pH were prepared (Section 2.5.1) and the solutions were monitored by UV–vis spectroscopy (Fig. S6a). No change in the intensity of 4-NP absorption peak (at 400 nm) was observed over time. This indicates a lack of 4-NP reduction in absence of **E2** at all pH ranges (Table S2). Adding the required quantity of **E2** to the reaction solution, the yellow color started to disappear (Fig. 6a) along with a decrease in the intensity of the 4-NP UV-absorption peak and the appearance of a new band at ~300 nm corresponding to 4-AP (Fig. 6b). The conversion and rate of reaction were determined from the intensity of the UV-absorption peak at 400 nm and given in Fig. S6b and Fig. 6c. $C_0$ and $C$ are the initial and residual concentrations of 4-NP at a given

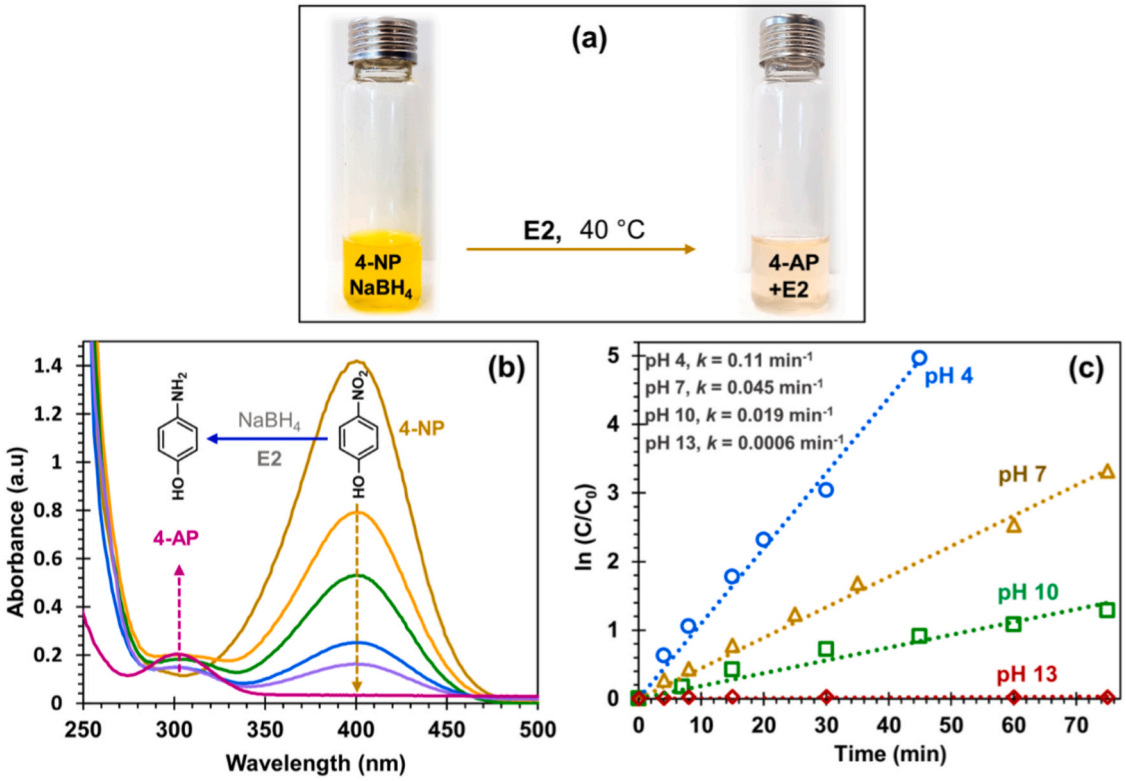


**Fig. 6.** (a) Change in color of 4-NP and $NaBH_4$ aqueous solution after reduction of 4-NP. The remaining light orange color is due to the presence of **E2** (b) UV–vis spectra recorded during the reduction of 4-NP at pH 4. (c) Effect of pH on the kinetics of 4-NP reduction by **E2**.

time, respectively.

Linear correlation between $-ln(C/C_0)$ vs. time indicates the pseudo-first-order reduction of 4-NP at all pH values (Fig. 6c), with a visible effect of pH on the rate of hydrogenation of 4-NP (Fig. 6c). The highest $k$ value at pH 4 (0.11 $min^{-1}$) followed by a decrease with an increase in pH (Fig. 6c) indicates the effect of deswelling of hydrogel matrix surrounding the AgNPs. Increasing the pH $\geq$ 12, a very low $k$ value (0.0006 $min^{-1}$) was observed, which signifies the lack of 4-NP hydrogenation (Fig. 6c and S6b). These observations, highlight the ability to control the activity of AgNPs by controlling the swelling of the microspheres. TOF of the 4-NP hydrogenation (at pH 4) was determined at different reaction duration (Fig. S6c) and was found to decrease with time, which is in agreement with earlier reports (Kozuch and Martin, 2012). TOF at full conversion was found to be ~170 $h^{-1}$ and ~100 $h^{-1}$ for pH 4 and 7 respectively (Table 2). TOFs achieved by **E2** at full conversion are higher than the recently reported state of art Au (Qin et al., 2019; Fu et al., 2018) and Ag (Zhou et al., 2020; Mao et al., 2018) based catalysts.

Based on the swelling behavior of composite microsphere and catalytic activity at different pH, a mechanism to explain the tunable behavior is proposed in Fig. 7. As observed during DLS analysis, **E2** reached a swollen state around pH 4, which coincides with the pH of the highest catalytic activity. This signifies the easy accessibility of AgNPs for the hydrogenation of 4-NP. Positive ζ-potential of **E2** at this pH (Table 1) also favors the adsorption of 4-NP and $BH_4^-$ on the catalyst. As a result, the local concentration of 4-NP and $BH_4^-$ around the microenvironment of AgNPs remains high and facilitates high catalytic activity. A similar strategy has been used to enhance the catalytic activity of Palladium/MOF catalysts for styrene hydrogenation (Huang et al., 2016). Additionally, pores of the hydrogel can also act like nano-reactors to enhance the activity via the well-known confined space reaction (Fig. 7) (Gong et al., 2019; Cárdenas-Lizana et al., 2013). A combination of these factors led to fast hydrogenation of 4-NP. Increasing the pH of the reaction medium decreased the access to AgNPs due to the deswelling of the **E2** (Fig. 7a). The decrease in ζ-potential (Table 1) with pH also reduces the local concentration of 4-NP. As a result, the catalytic reduction of 4-NP slowed down. Complete deswelling along with negative ζ-potential of **E2** above pH $\geq$ 12 block the access to AgNPs and, prevents any catalytic reduction (Figs. 6c, 7a).

### 3.4.2. Reduction of CR and MB

**E2** was also used for the reduction of pollutants of anionic (Congo red) and cationic (methylene blue) nature. The reduction pathway of carcinogenic azo dye like CR by AgNPs in the presence of $NaBH_4$ and AgNPs is well established and shown in Fig. S7a (Rajesh et al., 2014; Nasrollahzadeh et al., 2020). The residual CR in water is quantifiable by recording the UV–vis intensity of CR solution at different times (Fig S7b). Hydrogenation of CR under acidic medium (pH 4) was fast ($k$ = 1.8 $min^{-1}$) with a TOF of ~124 $h^{-1}$ (Fig. 8a, Table 2) highlighting the excellent activity of **E2**. The activity decreased with an increase in the pH and activity was turned OFF at pH 13 (Fig. 8a, S7c). Such behavior resembles the reduction of 4-NP and can be explained by Fig. 7a. In our previous study, we have shown that under an acidic medium this hydrogel favors adsorption of anionic dyes (Nazir et al., 2020b). Changing the pH to alkaline results in the repulsion of dye molecules from the hydrogel matrix (Nazir et al., 2020b). This behavior favors the adsorption of CR and faster degradation under an acidic medium. Repulsion between CR and hydrogel microsphere along with deswelling of **E2** prevents any degradation above pH 12.

**Table 2**
TOF obtained during the catalytic transformation of different molecules.

| Pollutant | TOF ($h^{-1}$) | pH |
|---|---|---|
| 4-NP | 170 | 4 |
| | 100 | 7 |
| CR | 124 | 4 |
| MB | 27 | 4 |

TOF = moles of molecules hydrogenated by one mole of Ag-atoms in 1 h. TOF values reported here are calculated at full conversion.

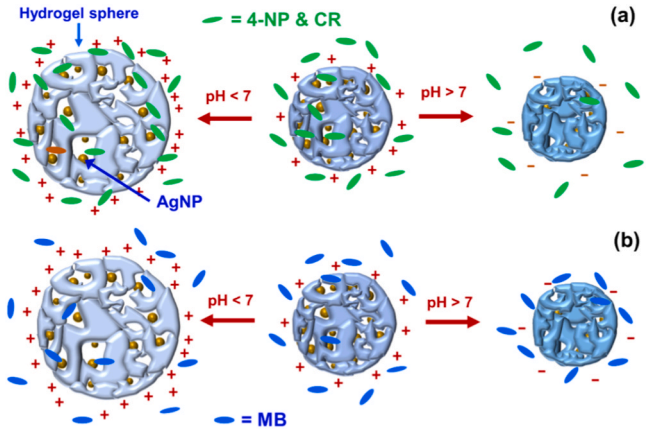


**Fig. 7.** Effect of pH on (a) distribution of 4-NP or CR and (b) MB in and around **E2** microspheres. Swelling and ζ-potential of **E2** at different pH controls the access to AgNP and local concentration of molecules.

During MB reduction, the highest catalytic activity was observed at pH 4 (Fig. 8b, S8) with a $k$ value of 0.52 $min^{-1}$, which is lower than the $k$-value observed during the reduction of 4-NP and CR. It is due to the decreased adsorption of cationic MB by the positively charged **E2** (Fig. 7b). As a result, the TOF of 27 $h^{-1}$ was observed during MB reduction at pH 4 (Table 2). On the contrary to 4-NP and CR hydrogenation, it was not possible to completely stop the hydrogenation of MB at pH 13. This can be explained as the adsorption and slow diffusion of MB molecules to reach AgNPs for catalysis owing to the negative surface charge of **E2** at pH 13 (Figs. 7b and 8b).

### 3.4.3. Selectivity and reusability

Differential catalytic reduction of cationic and anionic molecules by **E2** at pH $\geq$ 12 prompted the investigation of the substrate selective activity of the novel catalyst. A mixture of MB to 4-NP ($3 \times 10^{-4}$ mmol) maintained at pH 13 was subjected to hydrogenation. The green color of the solution slowly turned yellow (Fig. 9c), suggesting the selective reduction of only MB. UV–vis spectra of the solution also confirmed the hydrogenation of only MB (Fig. 9a, b). Interestingly, the concentration of 4-NP remained unchanged even after 3 h. This can be attributed to the selective and competitive adsorption of cationic MB molecules on **E2**, due to the negative surface charge at this pH.

To demonstrate the practical applicability, the catalyst **E2** was subjected to reuse cycles using 4-NP as a substrate. **E2** maintained its activity even after the fifth cycle (Fig. 9d) and activity could be turned OFF at the third cycle by raising the pH to 12. **E2** recovered its activity in the fourth cycle (at pH 4.5), highlighting the reversibility of its activity. No loss in catalytic activity after the fifth reuse cycle indicates easy recovery of **E2** and low loss of silver. Ag-content of 0.65 ± 0.06% determined by ICP-OES analysis after the fifth cycle confirmed a very low Ag loss (Table S1) and minimizes the risk of secondary pollution due to silver leaching from **E2**. Transmission images indicate hydrogel matrix successfully prevents agglomeration of AgNPs (Fig. S9), although some degree of agglomeration of hydrogel microspheres can be observed in Fig. S9. Agglomeration of microspheres can take place during sample preparation on a TEM grid or during catalyst recovery. From the catalyst reuse study, it is clear that such agglomeration is temporary and has no effect on its catalytic activity.

TOF of the novel catalyst (**E2**) calculated after 4-NP reduction (at pH 4) is superior to most of the recently reported AgNP-catalysts (Table 3, Entry 2–6). In the case of entry 7, excellent catalytic activity was

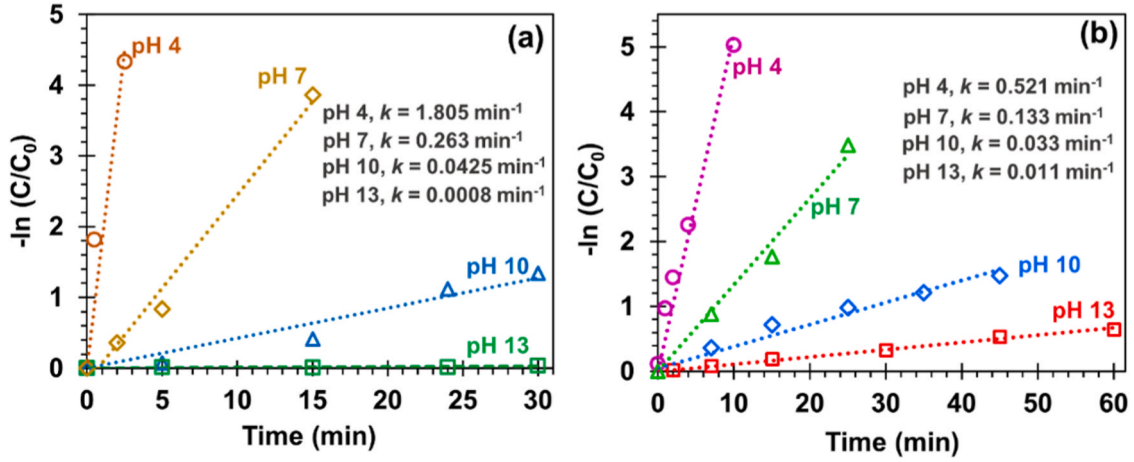


**Fig. 8.** Effect of pH on the kinetics of (a) CR and (b) MB reduction by **E2**. Insets in respective images show the values of reduction rate constant (*k*) at different pH.

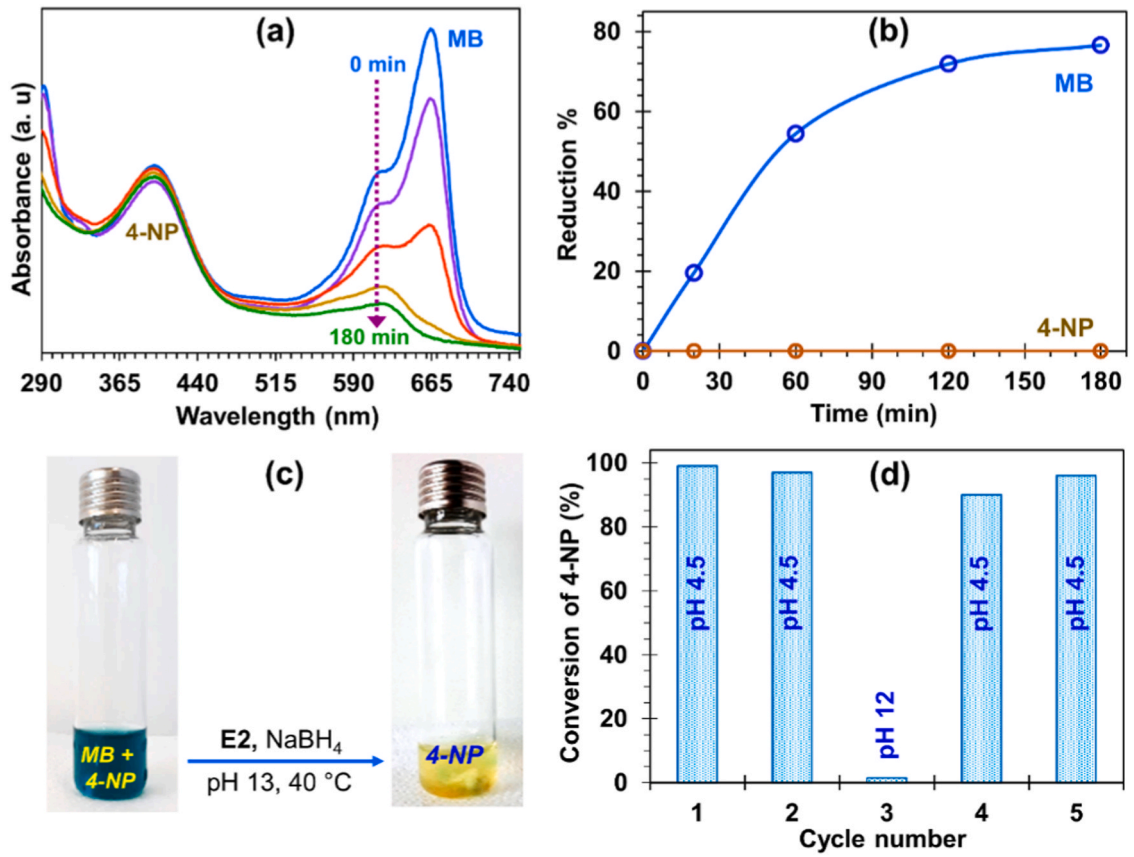


**Fig. 9.** Selective reduction of MB from the mixture of MB and 4-NP by **E2** at pH 13. Inset shows the change in color of the solution, marked as the reduction of only MB from the mixture. (d) Recycling of **E2** for catalytic hydrogenation of 4-NP showing the effect of pH. At cycle 3, pH 12 of the reaction medium turned off the catalytic activity of **E2** and achieved only 1.5% conversion.

reported for AgNP based catalysts, which is attributed to their ultrafine particle size and porous support. The catalyst prepared from an alloy of gold and silver also displayed lower TOF than **E2** (entry 8). AuNP based catalyst reported in entries 9 and 10 displayed significantly higher activity than **E2,** because of porous support that provides easy access to AuNPs and inherently high activity of AuNPs. Interestingly, **E2** requires a significantly lower quantity of $NaBH_4$ to achieve such high TOF compared to highly active catalysts listed in Table 3. Additionally, ease of controlling the activity and catalytic selectivity are distinct advantages of **E2** compared to the reported catalysts.

## 4. Conclusion

In summary, this work demonstrates a simple method to prepare AgNP based pH-responsive catalysts with excellent catalytic reduction of pollutants like 4-NP and dyes (CR and MB). The pH-responsive hydrogel support offers the possibility to control the access to AgNPs and the micro-environment around them, thereby tuning the catalytic activity. At its swollen state, AgNP-hydrogel-microsphere (**E2**) displayed an excellent catalytic reduction with TOF of 170 $h^{-1}$ and 124 $h^{-1}$ for 4-NP and CR respectively. Increasing the pH of the reaction media resulted

**Table 3**
The catalytic activity of the various catalyst for reduction of 4-NP to 4-AP.

| Entry | Catalyst | TOF ($h^{-1}$) | $NaBH_4$/4-NP (molar ratio) | Year | Ref. |
|---|---|---|---|---|---|
| 1 | AgNP-Hydrogel microsphere | 170 (pH 4), 100 (pH 7) | 9 | 2021 | This work |
| 2 | PAM/PPY/GO-Ag | 153.4 | 100 | 2018 | (Mao et al., 2018) |
| 3 | Microgel-stabilized AgNPs | 38 | 8 | 2019 | (Begum et al., 2019) |
| 4 | Ag/ZrGP catalyst | 1.0 | 1000 | 2020 | (Zhou et al., 2020) |
| 5 | AgNPs on COF | 81 | – | 2021 | (Wang et al., 2021) |
| 6 | Ag/Cu NPs supported on hollow $SiO_2$ sphere | 20 | 4 | 2021 | (Sun et al., 2021) |
| 7 | (a) Ultrafine AgNPs in cage type $SiO_2$ nanoparticles | 1164 | 100 | 2020 | (Budi et al., 2020) |
| | (b) Ultrafine Ni-Ag NPs in cage-type $SiO_2$ nanoparticles | 267 | 100 | 2020 | (Budi et al., 2020) |
| 8 | Au-Ag on PCP[a] | 130 | 30 | 2018 | (Fu et al., 2018) |
| 9 | Ni-Au-Carbon black | 214 | 50 | 2019 | (Qin et al., 2019) |
| 10 | $Fe_3O_4$@COF-Au | 354.6 | 440 | 2020 | (Xu et al., 2020) |

TOF = moles of 4-NP hydrogenated by one mole of Ag-atoms in 1 h.
Note: TOF was calculated using the data provided in the literature and at the completion of 4-NP reduction.
[a] PCP =multi-amino poly(cyclotriphosphazene-co-polyethyleneimine) (PCP) microspheres.

in a decrease in activity and was turned OFF once the pH was above 12. The composite catalyst also displayed a selective reduction of only MB at pH 13 from a mixture of MB and 4-NP, owing to the selective adsorption of MB (cationic pollutant) due to negative ζ-potential at this pH. Successful recyclability of this novel catalyst makes it suitable for various practical applications. Additionally, the substrate selectivity of this catalytic system can be utilized for further development of selective catalysts using other metals.

## CRediT authorship contribution statement

**Dambarudhar Parida:** Conceptualization; Methodology; Investigation; Data curation; Formal analysis; Supervision; Validation; Visualization; Writing - original draft; Writing - review & editing. **Eva Moreau:** Investigation; Data curation; Formal analysis. **Rashid Nazir:** Investigation. **Khalifah A. Salmeia:** Formal analysis; Writing - review & editing. **Ruggero Frison**: Investigation. **Ruohan Zhao**: Investigation. **Sandro Lehner:** Investigation. **Milijana Jovic:** Investigation. **Sabyasachi Gaan:** Methodology; Project administration; Resources; Supervision; Writing - review & editing.

## Declaration of Competing Interest

The authors declare that they have no known competing financial interests or personal relationships that could have appeared to influence the work reported in this paper.

## Acknowledgment

The authors thank Dr. Daniel Rentsch for the NMR analysis. We appreciate the support of Mr. Ton Markaj for ICP-OES analysis and the support of Dr. Roland Hauert for XPS analysis. The NMR hardware was partially granted by the Swiss National Science Foundation (SNSF, grant no. 206021_150638/1). The manuscript was written through the contribution of all and all authors have approved the final version of the manuscript.

## Appendix A. Supporting information

Supplementary data associated with this article can be found in the online version at doi:10.1016/j.jhazmat.2021.126237.

## References

Agnihotri, S., Mukherji, S., Mukherji, S., 2014. Size-controlled silver nanoparticles synthesized over the range 5–100 nm using the same protocol and their antibacterial efficacy. RSC Adv. 4, 3974–3983.
Ansar, S.M., Kitchens, C.L., 2016. Impact of gold nanoparticle stabilizing ligands on the colloidal catalytic reduction of 4-nitrophenol. ACS Catal. 6, 5553–5560.
Begum, R., Farooqi, Z.H., Aboo, A.H., Ahmed, E., Sharif, A., Xiao, J., 2019. Reduction of nitroarenes catalyzed by microgel-stabilized silver nanoparticles. J. Hazard. Mater. 377, 399–408.
Bhaduri, B., Polubesova, T., 2020. Facile synthesis of carbon-supported silver nanoparticles as an efficient reduction catalyst for aqueous 2-methyl-p-nitrophenol. Mater. Lett. 267, 127546.
Budi, C.S., Deka, J.R., Hsu, W.-C., Saikia, D., Chen, K.-T., Kao, H.-M., Yang, Y.-C., 2021. Bimetallic Co/Zn zeolitic imidazolate framework ZIF-67 supported Cu nanoparticles: an excellent catalyst for reduction of synthetic dyes and nitroarenes. J. Hazard. Mater. 407, 124392.
Budi, C.S., Deka, J.R., Saikia, D., Kao, H.-M., Yang, Y.-C., 2020. Ultrafine bimetallic Ag-doped Ni nanoparticles embedded in cage-type mesoporous silica SBA-16 as superior catalysts for conversion of toxic nitroaromatic compounds. J. Hazard. Mater. 384, 121270.
E.F.T.C.H. Buschmann, Analgesics and Antipyretics. In Ullmann's Encyclopedia of Industrial Chemistry, 2007.
Cárdenas-Lizana, F., Berguerand, C., Yuranov, I., Kiwi-Minsker, L., 2013. Chemoselective hydrogenation of nitroarenes: boosting nanoparticle efficiency by confinement within highly porous polymeric framework. J. Catal. 301, 103–111.
Cheng, X., Liu, M., Zhang, A., Hu, S., Song, C., Zhang, G., Guo, X., 2015. Size-controlled silver nanoparticles stabilized on thiol-functionalized MIL-53(Al) frameworks. Nanoscale 7, 9738–9745.
Coelho, A., 2018. TOPAS and TOPAS-Academic: an optimization program integrating computer algebra and crystallographic objects written in C++. J. Appl. Crystallogr. 51, 210–218.
Das, R., Sypu, V.S., Paumo, H.K., Bhaumik, M., Maharaj, V., Maity, A., 2019. Silver decorated magnetic nanocomposite (Fe3O4@PPy-MAA/Ag) as highly active catalyst towards reduction of 4-nitrophenol and toxic organic dyes. Appl. Catal. B Environ. 244, 546–558.
Dias, E.M., Petit, C., 2015. Towards the use of metal–organic frameworks for water reuse: a review of the recent advances in the field of organic pollutants removal and degradation and the next steps in the field. J. Mater. Chem. A 3, 22484–22506.
Dong, Z., Le, X., Li, X., Zhang, W., Dong, C., Ma, J., 2014. Silver nanoparticles immobilized on fibrous nano-silica as highly efficient and recyclable heterogeneous catalyst for reduction of 4-nitrophenol and 2-nitroaniline. Appl. Catal. B Environ. 158–159, 129–135.
Fu, Y., Qin, L., Huang, D., Zeng, G., Lai, C., Li, B., He, J., Yi, H., Zhang, M., Cheng, M., Wen, X., 2019. Chitosan functionalized activated coke for Au nanoparticles anchoring: green synthesis and catalytic activities in hydrogenation of nitrophenols and azo dyes. Appl. Catal. B Environ. 255, 117740.
Fu, J., Wang, S., Zhu, J., Wang, K., Gao, M., Wang, X., Xu, Q., 2018. Au-Ag bimetallic nanoparticles decorated multi-amino cyclophosphazene hybrid microspheres as enhanced activity catalysts for the reduction of 4-nitrophenol. Mater. Chem. Phys. 207, 315–324.
Fu, Y., Xu, P., Huang, D., Zeng, G., Lai, C., Qin, L., Li, B., He, J., Yi, H., Cheng, M., Zhang, C., 2019. Au nanoparticles decorated on activated coke via a facile preparation for efficient catalytic reduction of nitrophenols and azo dyes. Appl. Surf. Sci. 473, 578–588.
Goepel, M., Al-Naji, M., With, P., Wagner, G., Oeckler, O., Enke, D., Gläser, R., 2014. Hydrogenation of p-nitrophenol to p-aminophenol as a test reaction for the catalytic activity of supported Pt catalysts. Chem. Eng. Technol. 37, 551–554.
Gong, W., Wu, Q., Jiang, G., Li, G., 2019. Ultrafine silver nanoparticles supported on a covalent carbazole framework as high-efficiency nanocatalysts for nitrophenol reduction. J. Mater. Chem. A 7, 13449–13454.
Guenbour, A., Kacemi, A., Benbachir, A., 2000. Corrosion protection of copper by polyaminophenol films. Prog. Org. Coat. 39, 151–155.
Gupta, V.K., Kumar, R., Nayak, A., Saleh, T.A., Barakat, M.A., 2013. Adsorptive removal of dyes from aqueous solution onto carbon nanotubes: a review. Adv. Colloid Interface Sci. 193–194, 24–34.

Hoogesteijn von Reitzenstein, N., Bi, X., Yang, Y., Hristovski, K., Westerhoff, P., 2016. Morphology, structure, and properties of metal oxide/polymer nanocomposite electrospun mats, 133.
Huang, G., Yang, Q., Xu, Q., Yu, S.-H., Jiang, H.-L., 2016. Polydimethylsiloxane coating for a palladium/MOF composite: highly improved catalytic performance by surface hydrophobization. Angew. Chem. Int. Ed. 55, 7379–7383.
Irene, I.A., 2018. Vassalini, Switchable Stimuli-Responsive Heterogeneous Catalysis Catalysts, 8.
Johnson, J.A., Makis, J.J., Marvin, K.A., Rodenbusch, S.E., Stevenson, K.J., 2013. Size-dependent hydrogenation of p-nitrophenol with Pd nanoparticles synthesized with poly(amido)amine dendrimer templates. J. Phys. Chem. C 117, 22644–22651.
Ju, K.S., Parales, R.E., 2010. Nitroaromatic compounds, from synthesis to biodegradation. Microbiol. Mol. Biol. Rev. 74, 250–272.
Kästner, C., Thünemann, A.F., 2016. Catalytic reduction of 4-nitrophenol using silver nanoparticles with adjustable activity. Langmuir 32, 7383–7391.
Kozuch, S., Martin, J.M.L., 2012. "Turning over" definitions in catalytic cycles. ACS Catal. 2, 2787–2794.
Li, Y., Cao, Y., Xie, J., Jia, D., Qin, H., Liang, Z., 2015. Facile solid-state synthesis of Ag/graphene oxide nanocomposites as highly active and stable catalyst for the reduction of 4-nitrophenol. Catal. Commun. 58, 21–25.
Li, S., Ge, Y., Tiwari, A., Cao, S., 2010. A temperature-responsive nanoreactor. Small 6, 2453–2459.
Li, G.L., Tai, C.A., Neoh, K.G., Kang, E.T., Yang, X., 2011. Hybrid nanorattles of metal core and stimuli-responsive polymer shell for confined catalytic reactions. Polym. Chem. 2, 1368–1374.
Lu, Y., Mei, Y., Drechsler, M., Ballauff, M., 2006. Thermosensitive core–shell particles as carriers for Ag nanoparticles: modulating the catalytic activity by a phase transition in networks. Angew. Chem. Int. Ed. 45, 813–816.
Mao, H., Ji, C., Liu, M., Cao, Z., Sun, D., Xing, Z., Chen, X., Zhang, Y., Song, X.-M., 2018. Enhanced catalytic activity of Ag nanoparticles supported on polyacrylamide/polypyrrole/graphene oxide nanosheets for the reduction of 4-nitrophenol. Appl. Surf. Sci. 434, 522–533.
Marvin-Sikkema, F.D., de Bont, J.A., 1994. Degradation of nitroaromatic compounds by microorganisms. Appl. Microbiol Biotechnol. 42, 499–507.
Mishra, P.C., Mukherjee, S., Nayak, S.K., Panda, A., 2014. A brief review on viscosity of nanofluids. Int. Nano Lett. 4, 109–120.
Nasrollahzadeh, M., Jaleh, B., Baran, T., Varma, R.S., 2020. Efficient degradation of environmental contaminants using Pd-RGO nanocomposite as a retrievable catalyst. Clean. Technol. Environ. Policy 22, 325–335.
Nazir, R., Parida, D., Borgstädt, J., Lehner, S., Jovic, M., Rentsch, D., Bülbül, E., Huch, A., Altenried, S., Ren, Q., Rupper, P., Annaheim, S., Gaan, S., 2020. In-situ phosphine oxide physical networks: a facile strategy to achieve durable flame retardant and antimicrobial treatments of cellulose. Chem. Eng. J., 128028
Nazir, R., Parida, D., Guex, A.G., Rentsch, D., Zarei, A., Gooneie, A., Salmeia, K.A., Yar, K.M., Alihosseini, F., Sadeghpour, A., Gaan, S., 2020. Structurally tunable pH-responsive phosphine oxide based gels by facile synthesis strategy. ACS Appl. Mater. Interfaces 12, 7639–7649.
Nguyen, T.B., Huang, C.P., Doong, R.-A., 2019. Enhanced catalytic reduction of nitrophenols by sodium borohydride over highly recyclable Au@graphitic carbon nitride nanocomposites. Appl. Catal. B Environ. 240, 337–347.
Parida, D., Salmeia, K.A., Sadeghpour, A., Zhao, S., Maurya, A.K., Assaf, K.I., Moreau, E., Pauer, R., Lehner, S., Jovic, M., Cordula, H., Gaan, S., 2021. Template-free synthesis of hybrid silica nanoparticle with functionalized mesostructure for efficient methylene blue removal. Mater. Des. 201, 109494.
Parida, D., Simonetti, P., Frison, R., Bülbül, E., Altenried, S., Arroyo, Y., Balogh-Michels, Z., Caseri, W., Ren, Q., Hufenus, R., Gaan, S., 2020. Polymer-assisted in-situ thermal reduction of silver precursors: a solventless route for silver nanoparticles-polymer composites. Chem. Eng. J. 389, 123983.
Piao, L.L., Hoon, Kyung, Mn, Koun, Byoung, Woong, Kim, Young Rag, Do, Sungho, Yoon, 2011. A facile synthetic method of silver nanoparticles with a continuous size range from sub-10 nm to 40 nm. Bull. Korean Chem. Soc. 32, 117–121.
Qian, Y., Zhou, C., Zhou, J., Huang, A., 2020. Synthesis of silver-nanoparticles composite with highly catalytic activity supported on the reduced graphene oxide. Appl. Surf. Sci. 525, 146597.
Qin, L., Zeng, Z., Zeng, G., Lai, C., Duan, A., Xiao, R., Huang, D., Fu, Y., Yi, H., Li, B., Liu, X., Liu, S., Zhang, M., Jiang, D., 2019. Cooperative catalytic performance of bimetallic Ni-Au nanocatalyst for highly efficient hydrogenation of nitroaromatics and corresponding mechanism insight. Appl. Catal. B Environ. 259, 118035.
Rajesh, R., Kumar, S.S., Venkatesan, R., 2014. Efficient degradation of azo dyes using Ag and Au nanoparticles stabilized on graphene oxide functionalized with PAMAM dendrimers. N. J. Chem. 38, 1551–1558.
Ruíz-Baltazar, Ád.J., Reyes-López, S.Y., Mondragón-Sánchez, Md.L., Estevez, M., Hernández-Martinez, A.R., Pérez, R., 2018. Biosynthesis of Ag nanoparticles using Cynara cardunculus leaf extract: evaluation of their antibacterial and electrochemical activity. Results Phys. 11, 1142–1149.
Sirohi, S., Mittal, A., Nain, R., Jain, N., Singh, R., Dobhal, S., Pani, B., Parida, D., 2019. Effect of nanoparticle shape on the conductivity of Ag nanoparticle poly(vinyl alcohol) composite films. Polym. Int. 68, 1961–1967.
Soğukömeroğulları, H.G., Karataş, Y., Celebi, M., Gülcan, M., Sönmez, M., Zahmakiran, M., 2019. Palladium nanoparticles decorated on amine functionalized graphene nanosheets as excellent nanocatalyst for the hydrogenation of nitrophenols to aminophenol counterparts. J. Hazard. Mater. 369, 96–107.
Sudhakar, P., Soni, H., 2018. Catalytic reduction of Nitrophenols using silver nanoparticles-supported activated carbon derived from agro-waste. J. Environ. Chem. Eng. 6, 28–36.
Sun, J., Fu, Y., He, G., Sun, X., Wang, X., 2014. Catalytic hydrogenation of nitrophenols and nitrotoluenes over a palladium/graphene nanocomposite. Catal. Sci. Technol. 4, 1742–1748.
Sun, D., Yin, Z., Zeng, W., Cao, S., 2021. Bimetallic Ag/Cu supported hollow SiO2 sphere drives the efficient hydrogenation of nitroarenes. J. Solid State Chem. 297, 122052.
Thenmozhi, G., Arockiasamy, P., Santhi, R.J., 2014. Isomers of poly aminophenol: chemical synthesis, characterization, and its corrosion protection aspect on mild steel in 1 M HCl. Int. J. Electrochem. 2014, 1–11.
Wang, N., Wang, F., Pan, F., Yu, S., Pan, D., 2021. Highly efficient silver catalyst supported by a spherical covalent organic framework for the continuous reduction of 4-nitrophenol. ACS Appl. Mater. Interfaces 13, 3209–3220.
Wang, Y., Yan, R., Zhang, J., Zhang, W., 2010. Synthesis of efficient and reusable catalyst of size-controlled Au nanoparticles within a porous, chelating and intelligent hydrogel for aerobic alcohol oxidation. J. Mol. Catal. A Chem. 317, 81–88.
Xia, J., He, G., Zhang, L., Sun, X., Wang, X., 2016. Hydrogenation of nitrophenols catalyzed by carbon black-supported nickel nanoparticles under mild conditions. Appl. Catal. B Environ. 180, 408–415.
Xu, Y., Shi, X., Hua, R., Zhang, R., Yao, Y., Zhao, B., Liu, T., Zheng, J., Lu, G., 2020. Remarkably catalytic activity in reduction of 4-nitrophenol and methylene blue by Fe3O4@COF supported noble metal nanoparticles. Appl. Catal. B Environ. 260, 118142.
Yagub, M.T., Sen, T.K., Afroze, S., Ang, H.M., 2014. Dye and its removal from aqueous solution by adsorption: a review. Adv. Colloid Interface Sci. 209, 172–184.
Yang, Y., Jiang, K., Guo, J., Li, J., Peng, X., Hong, B., Wang, X., Ge, H., 2020. Facile fabrication of Au/Fe3O4 nanocomposites as excellent nanocatalyst for ultrafast recyclable reduction of 4-nitropheol. Chem. Eng. J. 381, 122596.
Zeng, T., Zhang, X.-l, Niu, H.-Y., Ma, Y.-R., Li, W.-H., Cai, Y.-Q., 2013. In situ growth of gold nanoparticles onto polydopamine-encapsulated magnetic microspheres for catalytic reduction of nitrobenzene. Appl. Catal. B Environ. 134–135, 26–33.
Zhao, H., Song, F., Zhang, J., Wang, F., Liu, J., Liu, Y., 2013. Fluorescence quenching of osthole by silver nanoparticles. J. Opt. Soc. Am. B 30, 2387–2392.
Zheng, P., Zhang, W., 2007. Synthesis of efficient and reusable palladium catalyst supported on pH-responsive colloid and its application to Suzuki and Heck reactions in water. J. Catal. 250, 324–330.
Zhou, A., Li, J., Wang, G., Xu, Q., 2020. Preparation of Ag/ZrGP nanocomposites with enhanced catalytic activity for catalytic reduction of 4-nitrophenol. Appl. Surf. Sci. 506, 144570.